

Excess current in single wall carbon nanotube weak links in the Fabry-Perot regime

H. Ingerslev Jørgensen^{†,*}, K. Grove-Rasmussen[†], and P.E. Lindelof

Nano-Science Center, Niels Bohr Institute,

University of Copenhagen, Denmark

[†] *These authors contributed equally to this work*

(Dated: December 2, 2024)

Abstract

We have for the first time succeeded in making reproducible high transparency superconducting contacts to gated single-walled carbon nanotubes (SWCNTs). The electrodes consist of superconducting Ti/Al/Ti trilayers. The here reported semiconducting SWCNT has high transparency contacts with a normal state differential conductance close to $4e^2/h$, and clear Fabry-Perot interference patterns in bias the spectroscopy plot. We observe peaks in the differential conductance at $\pm 2\Delta/e$ due to the onset of quasi particle tunneling, and features at $\pm\Delta/e$ and $\pm 2\Delta/3e$ due to multiple Andreev reflections. A peak in the conductance at zero bias might reflect a supercurrent. An excess current is observed and extracted at several different gate voltages. The dependence of the excess current on normal state conductance is presented and fitted to SNS-theory with good agreement.

PACS numbers: Valid PACS appear here

*Electronic address: hij@fys.ku.dk

Electron transport through a SWCNT bridging two metal electrodes has been studied intensively over the last years. At low temperatures different transport regimes depending on the transparency of the metal-SWCNT interfaces have been identified. With low transparency contacts a quantum dot (QD) will be defined in the SWCNT [1, 2, 3, 4], and with intermediate transparency contacts Kondo resonances around zero bias are observed [5, 6]. High transparency contacts are in recent years also reported, where the SWCNT constitutes an electron waveguide with Fabry-Perot (FP) interferences [7, 8].

A carbon nanotube (CNT) as the normal material in a SNS Josephson junction has been studied for multi wall CNTs [9, 10, 11, 12] and SWCNTs [13, 14], but to our knowledge not in the high transparency regime with FP interferences. A higher proximity induced supercurrent than theoretically predicted has also been observed for a SWCNT without a gate [15]. In this letter we will present transport measurements on a gated S-SWCNT-S Josephson junction at low temperatures, with high transparency contacts each consisting of a superconducting trilayer of Ti/Al/Ti.

The SWCNTs are grown by chemical vapor deposition (CVD) from catalyst islands made by electron beam lithography and positioned relative to predefined alignment marks. The details of the CVD-growth procedure are described elsewhere [14, 16]. After growth, source and drain electrodes consisting of superconducting trilayers are positioned next to the catalyst islands to contact the SWCNT. The gap between the source and drain trilayer films is approximately 500nm . The superconducting trilayers consist of 5nm titanium to make good contact to the SWCNT, then of 40nm aluminum to raise the transition temperature, and finally 5nm titanium to stop oxidation of the aluminum.

Our devices are made on a highly doped silicon wafer with a $0.5\mu\text{m}$ thermally oxidized SiO_2 layer on top. We use the silicon substrate as a back gate.

To be able to measure the transition temperature T_C and the critical field B_C of the trilayer films at low temperatures we furthermore define a four probe device of the superconducting trilayer. For the device in this letter we find $T_C = 750\text{mK}$, $B_C = 75\text{mT}$ and from BCS theory we calculate a superconducting energy gap of $2\Delta = 3.5k_B T_C = 230\mu\text{eV}$.

All measurements are preformed at 300mK in a sorption pumped ^3He cryostat (Oxford Instruments Heliox). The measurements are made with standard DAQ cards, lock-in amplifiers (excitation $5\mu\text{V}$), and opto-couplers to reduce noise.

Figure 1 shows a gatesweep from -10V to 0V with $V_{sd} = 1\text{mV}$ ($> 2\Delta/e$). It displays strong

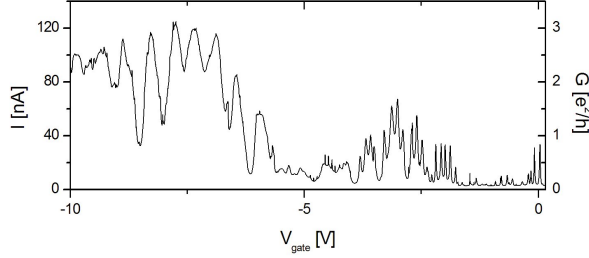


FIG. 1: Current and linear conductance are plotted for the S-SWCNT-S Josephson junction as function of voltage applied to the back gate with 1mV source drain voltage. The high conductance regime with Fabry-Perot oscillations is reached at large negative gate voltages ($< -6V$). Coulomb blockade peaks are seen at lower gate voltages.

gate dependence: High linear conductance at high negative gate voltages and low linear conductance at small gate voltages. This indicates that the SWCNT is semiconducting and the measurements are of transport through the valence band.

Because the Schottky barriers at the electrode-SWCNT interfaces are gate dependent, the device can be tuned from a QD with large Schottky barriers to an almost open 1D channel with negligible Schottky barriers.

From $V_{gate} \sim -4V$ to $V_{gate} \sim -2V$ the device is in the QD regime, where Coulomb Blockade peaks are clearly visible. Some of them are spaced into periods of four due to spin and orbital degeneracy of the SWCNT confirmed by bias spectroscopy plots (not shown). Such characteristic is sign of a high quality SWCNT. We will not go into further details about measurements made in the QD region, instead we now turn our attention to the regime of high conductance from $V_{gate} = -10V$ to $V_{gate} = -6.5V$.

Figure 2(a) shows a bias spectroscopy plot of this gate region with a small magnetic field applied ($B = 100mT$) to suppress the superconducting state of the electrodes.

The average differential conductance in this gate region is around $\sim 2.5e^2/h$ with maximums of about $\sim 3e^2/h$, approaching the theoretical limit of $4e^2/h = (6.5k\Omega)^{-1}$. Compared to the QD-regime described above, holes are now transported coherently through the SWCNT with only little reflection at the electrode-SWCNT interfaces. As V_{gate} and V_{sd} are changed the dips in conductance evolve into straight lines, forming a mesh of crossing dark lines (indicated with black lines in figure 2(a)). These pronounced oscillations in differential conductance versus V_{gate} and V_{sd} are clear signs of FP interference of electron waves that

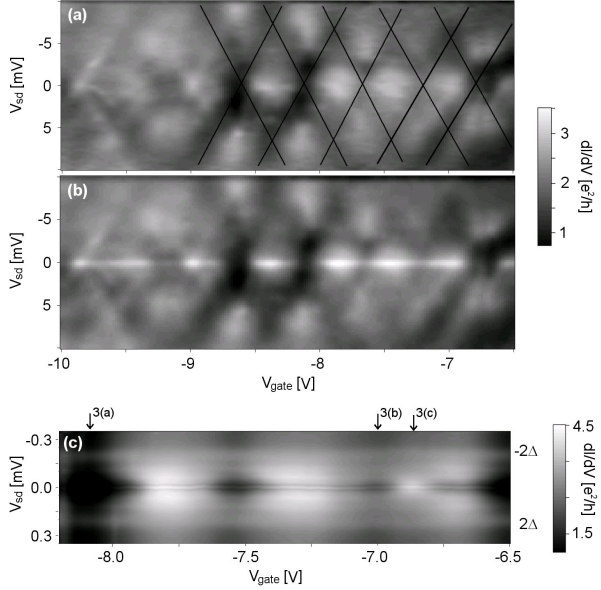


FIG. 2: (a) shows a bias spectroscopy plot in the high transparency gate region, with a small magnetic field ($B = 100\text{mT}$) to suppress the superconducting state of the electrodes. The black lines indicate the Fabry-Perot pattern. (b) is analog to (a) but without magnetic field, i.e. with superconducting electrodes. In (c) we show a zoom-in around small source drain voltages where the excess current is observed. Arrows are pointing to the gate voltages where the graphs in figure 3(a-c) are measured.

are reflected back and forth at the electrode-SWCNT interfaces [7].

As we turn off the magnetic field, i.e. turn on the superconducting state of the electrodes, an overall increase in differential conductance between $V_{sd} \sim \pm 2\Delta/e$ is observed. A bias spectroscopy plot of this overall increase is shown in figure 2(c). As will be described in more detail below this increase includes a rich sub gap structure.

Detailed measurements with lock-in amplifier of differential conductance versus V_{sd} at gate voltages indicated in figure 2(c) are shown in figure 3(a-c), where (a) and (b) are through two antiresonances of the FP pattern with a large difference in normal state differential conductance (G_N) and (c) is through a resonance.

The conductance increase between $V_{sd} \sim \pm 2\Delta/e$ is seen for most gate voltages, but a dip also always develops at smaller source drain voltages. In figure 3(b) this dip can be seen between $V_{sd} \sim \pm 80\mu\text{V}$ and more strongly in figure 3(a) where the dip evolves down below

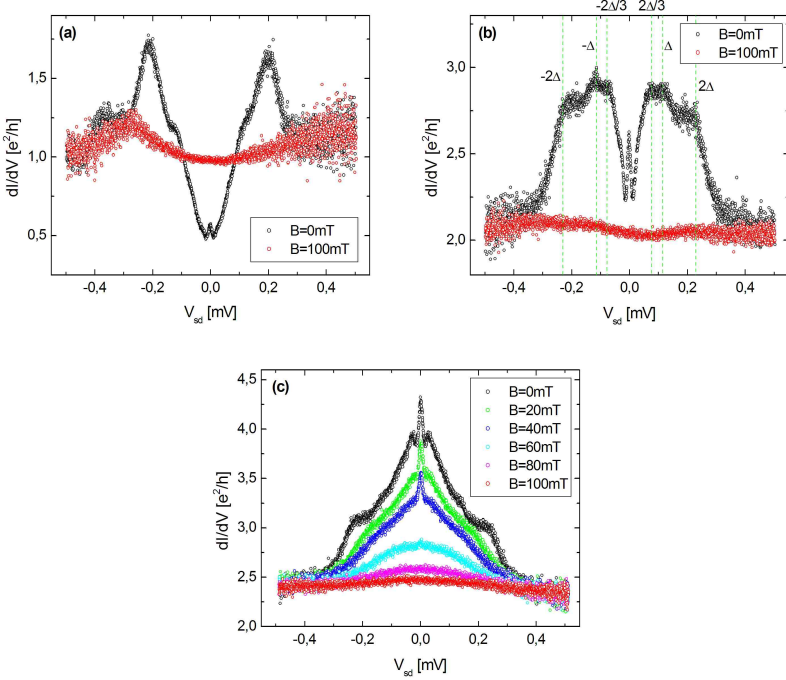


FIG. 3: Differential conductance versus source drain voltage measured with lock-in amplifier ($5\mu V$ excitation) at different gate voltages as indicated in figure 2(c). Black is with superconducting electrode and red is with $100mT$ magnetic field to suppress the superconductivity of the electrodes. (a) and (b) are measured at two different antiresonances of the Fabry-Perot pattern and (c) is measured at a resonance with increasing magnetic fields applied. Development from tunnel-like characteristic in (a) with relative low conductance towards an open 1D channel in (c) with high conductance is seen.

G_N . Similar strong dips are also observed at $V_{gate} = -6.5V$ and $V_{gate} = -8.7V$. The change in conductance between $V_{sd} \sim \pm 2\Delta/e$ to typically higher, but also lower values than G_N , is because superconductivity induced transport mechanisms occur.

Between $V_{sd} \sim \pm 2\Delta/e$ transport is governed by Andreev reflections (ARs) [17]. Since no single particle states exist below the superconducting gap no single particle tunneling is allowed. An electron with energy $|\epsilon| < \Delta$ relative to the Fermi energy in the normal region has a probability depending on the barrier strength (Z) for being AR on the superconductor as a hole effectively transferring two electrons (one Cooper pair) through the NS interface [18, 19]. For $|\epsilon| > \Delta$ the probability for ARs falls off rapidly, and we will therefore in the following neglect such ARs. Multiple Andreev reflections (MARs) will at finite bias give

rise to a subgap structure [20, 21], while at zero bias ARs set up bound states that carry a supercurrent providing that the interfaces are sufficiently transparent.

In figure 3(b) we observe features at $V_{sd} = \pm 2\Delta/en$ for $n = 1, 2, 3$, and a peak around zero bias, which is a general trend in our S-SWCNT-S junctions with high transparency. At $V_{sd} \gg 2\Delta/e$ transport is due to normal transport and the FP pattern is seen (processes with one AR are also allowed, but not dominant). As we approach $V_{sd} = 2\Delta/e$ the electron transport will be changed due to the modified DOS of the superconductor. At $V_{sd} = 2\Delta/e$ a conductance peak due to quasiparticle tunneling is seen because the peaks in the DOS of source and drain are aligned.

When the source drain voltage is lowered to $2\Delta/e > V_{sd} > \Delta/e$, a change in transport occurs. Direct tunneling of quasiparticles is no longer possible, instead transport is governed by one and two ARs. At $V_{sd} = \Delta/e$ a conductance peak is seen because the peaked DOS of source and drain each enhances a one AR process.

As V_{sd} is lowered further to $\Delta/e > V_{sd} > 2\Delta/3e$ transport changes again. Transport governed by one AR is no longer allowed whereas transport governed by two and three ARs are possible. At $V_{sd} \sim 2\Delta/3e$ a new conductance peak is seen because the peaked DOS of source and drain enhances transport governed by two ARs.

At even lower source drain voltages higher order MARs are expected. Features of these MARs can no longer be seen in our junctions, but since the differential conduction still increases below $V_{sd} = 2\Delta/3e$ in figure 3(c) higher order MARs ($n > 3$) are contributing.

For several of our high transparency S-SWCNT-S junctions we have observed that all these MARs give rise to a positive excess current that depends on G_N . In the following we will characterize the junction by its excess current. Excess current I_{exc} is defined as the difference in current between having the electrodes in the superconducting state and the normal state at $V_{sd} \gg \Delta/e$. It can therefore be found as half of the difference in area between the black and red curves in figure 3(a-c).

In figure 3(c) we show dI/dV versus V_{sd} through a resonance with increasing magnetic fields applied. The excess current is extracted as just described and plotted as a function of the magnetic field in figure 4(b). It shows a very clear linear decrease as the magnetic field is increased, with zero excess current close to $B_C = 75mT$.

In the inset of figure 4(a) we have extracted the excess currents at several different gate voltages in the FP region and plotted them against G_N that gate voltage. It shows

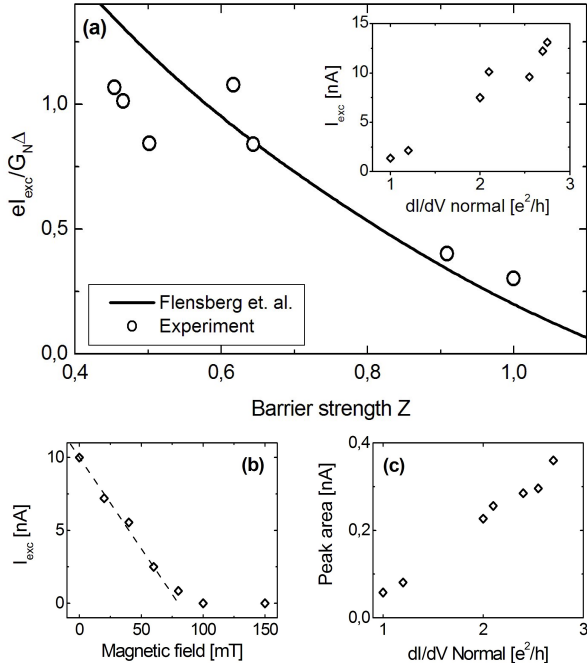


FIG. 4: In (a) the excess current is plotted in units of $eI_{exc}/G_N\Delta$ versus scattering parameter Z . Each of the experimental points (circles) are extracted at different gate voltages. The solid line is the theoretically predicted excess current for a 1D system connected to superconductors with adjustable scattering strength (Z) of the barriers [22]. No fitting parameter is used to obtain the good agreement between our data and the theory. The inset shows the same extracted excess currents as function of normal state differential conduction. In (b) we show the excess current versus applied magnetic field (dashed line is a guideline to the eye) and (c) shows the zero bias peak area versus normal state differential conductance.

that the excess current increases linearly with G_N , with a maximum of about $15nA$. A higher G_N means that the barrier strength is lower which gives a higher probability for the incoming electron on the superconductor to be AR instead of normal reflected thus yielding an increasing excess current [18]. In figure 4(a) we plot the same extracted excess currents in units of $eI_{exc}/G_N\Delta$ versus barrier strength Z , which relate to G_N as $G_N = 4e^2/h \cdot (1/(1+Z^2))^2$ [21, 22]. The solid line is a theoretically calculated excess current for a 1D system connected to superconductors by Flensberg et. al. [22]. Delta function barriers at the interfaces are included in the theory through the barrier strength parameter Z . Considering that there are no fitting parameter in the theory we see a very

good agreement between our experimentally measured excess current and the theoretical calculation. The excess current of our S-SWCNT-S nanotube can thus be described well by SNS theory.

Around zero bias with a full width of only $\sim 25\mu V$ a clear conductance peak is observed (figure 3(a-c)), which persists at all gate voltages in the FP-region. This zero bias peak might be due to a supercurrent [14], which agrees with its maximum reaching higher than $4e^2/h$ in all of the resonances in figure 2(c). However, if this is the case some smearing of the peak must be present since the peak does not reach the value of the series conductance of our measurement setup $\sim (100\Omega)^{-1}$. To characterize this possible supercurrent we therefore estimate its magnitude in accordance with the RSJ model as the area of the peak (not the whole area under the peak since the voltage dependent resistor in the RSJ model includes all normal current as well as current due to the MARs at finite biases). In figure 4(c) we plot this peak area versus G_N , where each data point is obtained at different gate voltages. It shows that the possible supercurrent increases linearly with G_N with a maximum of only $0.4nA$. Similar peaks at zero bias with area $\lesssim 1nA$ are also seen in other devices. The linear increase agrees with the dependence of the theoretically expected supercurrent for a SNS junction $I_S = (\pi\Delta/e) \cdot G_N$, but the magnitude is about two orders of magnitude lower, $I_S = 40nA$ for $G_N = 3e^2/h$. The theoretically expected supercurrent is of the same order of magnitude as the extracted excess current but we do not understand why the measured supercurrent is so much lower.

We have in another device with lower transparency observed a dramatic increase of the peak area as function of temperature below $100mK$ [14]. A similar behavior could therefore be expected for the here reported device, and thus explain the peak area as a not fully developed supercurrent.

In conclusion we have for the first time successfully fabricated gated S-SWCNT-S Josephson junctions with high transparency contacts. In the FP regime of the here reported semiconducting SWCNT we observe quasiparticle tunneling at $V_{sd} = 2\Delta/e$, features of MARs at $V_{sd} = 2\Delta/en$ for $n = 2, 3$, and a conductance peak around zero bias. The zero bias conduction peak might be due to a not fully developed supercurrent. The excess current which has not been analyzed before for such junctions scales linearly with the normal conductance of the junction and fits very well to theory for SNS junctions.

Acknowledgments

We wish to acknowledge the support of the Danish Technical Research Council (The Nanomagnetism framework program), EU-STREP Ultra-1D program and the Nano-Science Center, University of Copenhagen, Denmark.

- [1] S. Tans, M. H. Devoret, H. Dai, A. Thess, R. E. Smalley, L. J. Geerligs, and C. Dekker, *Nature* **386**, 474 (1997).
- [2] M. Bockrath, D. H. Cobden, P. L. McEuen, N. G. Chopra, A. Zettl, A. Thess, and R. E. Smalley, *Science* **275**, 1922 (1997).
- [3] D. H. Cobden and J. Nygård, *Phys. Rev. Lett.* **89**, 046803 (2002).
- [4] P. J. Herrero, S. Sapmaz, C. D. L. P. Kouwenhoven, and H. S. van der Zant, *Nature* **429**, 389 (2004).
- [5] J. Nygård, D. H. Cobden, and P. E. Lindelof, *Nature* **408**, 342 (2002).
- [6] B. Babic, T. Kontos, and C. Schönenberger, *Phys. Rev. B* **70**, 235419 (2004).
- [7] W. Liang, M. Bockarth, D. Bozovic, J. H. Hafner, M. Tinkham, and H. Park, *Nature* **411**, 665 (2001).
- [8] J. Cao, Q. Wang, M. Rolandi, and H. Dai, *Phys. Rev. Lett.* **93**, 216803 (2004).
- [9] M. R. Buitelaar, W. Belzig, T. Nussbaumer, B. Babic, C. Bruder, and C. Schönenberger, *Phys. Rev. Lett.* **91**, 057005 (2003).
- [10] M. R. Buitelaar, T. Nussbaumer, and C. Schönenberger, *Phys. Rev. Lett.* **89**, 256801 (2002).
- [11] E. Vecino, M. Buitelaar, A. Martin-Rodero, C. Schönenberger, and A. L. Yeyati, *Phys. Rev. Lett.* **89**, 256801 (2002).
- [12] J. Haruyama, K. Takazawa, S. Miyadai, A. Takeda, N. Hori, I. Takesue, Y. Kanda, N. Sugiyama, T. Akazaki, and H. Takayanagi, *Phys. Rev. B* **68**, 165420 (2003).
- [13] A. F. Morpurgo, J. Kong, C. M. Marcus, and H. Dai, *Science* **286**, 263 (1999).
- [14] K. Grove-Rasmussen, H. I. Jørgensen, and P. E. Lindelof, *Results to be published* (2005).
- [15] A. Y. Kasumov, R. Deblock, M. Kociak, B. Reulet, H. Bouchiat, I. I. Khodos, Y. B. Gorbatov, V. T. Volkov, C. Journet, and M. Burghard, *Science* **284**, 1508 (1999).
- [16] J. Kong, H. T. Soh, A. M. Cassell, C. F. Quate, and H. Dai, *Nature* **395**, 878 (1998).

- [17] A.F. Andreev, *Zh. Eksp. Theor. Fiz.* **46**, 1823 (1964).
- [18] G. E. Blonder, M. Tinkham, and T. M. Klapwijk, *Phys. Rev. B* **25**, 4515 (1982).
- [19] T. M. Klapwijk, M. Tinkham, and G. E. Blonder, *Physica B+C* **109-110**, 1657 (1982).
- [20] P. E. Gregers-Hansen, E. Hendricks, M. T. Levinsen, and G. R. Pickett, *Phys. Rev. Lett.* **31**, 524 (1973).
- [21] M. Octavio, G. E. Blonder, M. Tinkham, and T. M. Klapwijk, *Phys. Rev. B* **27**, 6739 (1983).
- [22] K. Flensberg, J. B. Hansen, and M. Octavio, *Phys. Rev. B* **38**, 8707 (1988).